Journal of
Materials Chemistry A

Accepted Manuscript

This article can be cited before page numbers have been issued, to do this please use: J. R. Peet, M. S. Chambers, A. Piovano, M. Johnson and I. R. Evans, *J. Mater. Chem. A*, 2018, DOI: 10.1039/C8TA00546J.

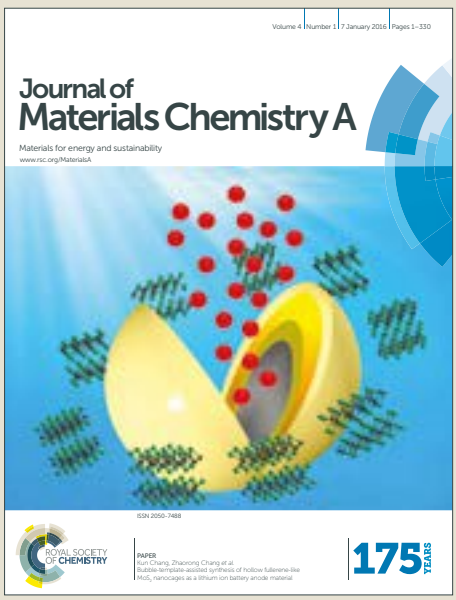

ROYAL SOCIETY OF CHEMISTRY

rsc.li/materials-a

View Article Online
DOI: 10.1039/C8TA00546J

Journal Name

ARTICLE

Dynamics in Bi(III)-containing Apatite-Type Oxide Ion Conductors: A Combined Computational and Experimental Study

Received 00th January 20xx,
Accepted 00th January 20xx

DOI: 10.1039/x0xx00000x

www.rsc.org/

J. R. Peet,[a,b] M. S. Chambers, [a,c] A. Piovano[b] , M. R. Johnson[b] and I. Radosavljevic Evans[a,*]

Introduction of Bi(III) into apatite-type germanate oxide ion conductors can improve the conductivity by up to two orders of magnitude. To account for these experimental findings, we have carried out the first *ab initio* molecular dynamics simulations study of the conduction mechanisms in lone pair-containing apatite-type oxide ion conductors. These calculations were performed on the series $La_{10-x}Bi_xGe_6O_{27}$ (x=0, 2, 4) and were supported by neutron scattering experiments. We observe four types of oxide ion exchange mechanisms and describe the effects that the introduction of lone-pair cations has on the O^{2-} migration pathways and on the overall conductivity .

Introduction

Oxide ion conductors are of considerable interest due to their range of environmental and energy-related applications including oxygen sensors and pumps,[1] separation membranes,[2, 3] and as electrolytes in solid oxide fuel cells (SOFCs).[4-6] Understanding the dynamics and the conduction pathways in these materials in relation to their structural characteristics is a key requirement for improving their properties through smart design.[7-13]

One group of solid electrolytes of particular interest due to high oxide ion conductivities are apatite-type materials, especially lanthanum silicates and germanates.[14-19] Conductivities have been reported reaching up to 6×10^{-2} S cm^{-1} at 800 °C for the mixed silicate-germanate $La_{9.33}Si_2Ge_4O_{26}$ composition,[20] with high intermediate-temperature conductivities also reported (e.g. 3×10^{-3} S/cm at 500 °C for $La_{9.67}Si_{5.5}Mg_{0.5}O_{26}$). [21]

Apatites are chemically flexible materials with general formula $A_{10}(TO_4)_6X_{2\pm\delta}$, (A = 2+ or 3+ cation; T = Si^{4+}, Ge^{4+}, V^{5+}, P^{5+}; X = O^{2-}, halide, OH^-), that generally adopt a hexagonal $P6_3/m$ structure.[22] The structure of apatite oxide materials with formula $A_{10}(TO_4)_6O_2$ comprises two crystallographically distinct A sites (referred to as A1 and A2), a tetrahedrally coordinated T site and four unique O sites (referred to as O1-O4), Fig. 1. The polyhedral connectivity is such that the $A_4(TO_4)_6$ framework (involving the A1, T and O1-O3 sites) forms channels along the *c* crystallographic direction, and these channels are occupied by A_6O_2 units (involving the A2 and O4 sites). For compositions with more than 26 O atoms per formula unit, the structure contains an additional interstitial oxygen site, the location of which has been the subject of much debate and may vary depending on exact composition.[23-30]

Recently, a combination of high-resolution neutron powder diffraction and aberration-corrected scanning transmission electron microscopy confirmed the presence of interstitial O atoms (O5 sites) between the GeO_4 tetrahedra (red circles in Fig. 1, effectively forming GeO_5 groups), as well as the presence of Bi on the A2 crystallographic sites in $La_8Bi_2(GeO_4)_6O_3$, triclinically distorted apatite-type oxide ion conductor.[30]

The ionic conductivity of $La_8Bi_2(GeO_4)_6O_3$ is about half an order of magnitude higher than that of $La_{10}(GeO_4)_6O_3$ (1.3×10^{-2} S/cm and 7.8×10^{-3} S/cm at 775°C, respectively).[31] Similarly, other related pairs of pure-La and Bi-containing germanates exhibit the same trend. For example, the ionic conductivities of $La_8Ba_2(GeO_4)_6O_2$ and $La_6Bi_2Ba_2(GeO_4)_6O_2$ at 800°C were reported as 5.5×10^{-5} S/cm and 1×10^{-3} S/cm, respectively, and 5.3×10^{-5} S/cm and 3×10^{-3} S/cm for $La_8Sr_2(GeO_4)_6O_2$ and $La_6Bi_2Sr_2(GeO_4)_6O_2$.[32, 33] Understanding the role of Bi in enhancing conductivity is one of the aims of this paper.

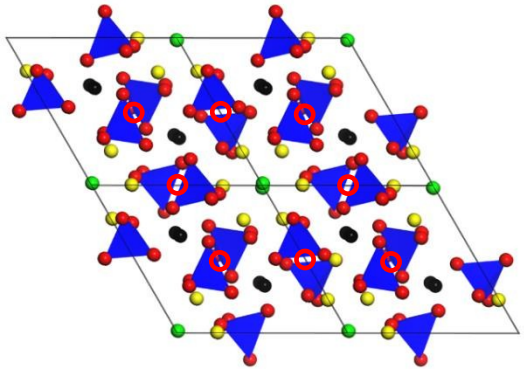

Figure 1: Structure of a hexagonal apatite material with general formula $A_{10}(TO_4)_6O_2$. Black spheres represent A1 as part of an $A_4(TO_4)_6$ framework with blue tetrahedra representing the TO_4 groups, and red spheres the O1, O2 and O3 sites. Yellow spheres represent A2 sites that make up A_6O_2 units that lie within channels formed by this framework. Green spheres represent the O4 sites (or X, which may be halide, hydroxide or vacant, depending on composition). Red circles indicate the locations of the interstitial oxygen atoms (O5) in hexagonal $La_8Bi_2(GeO_4)_6O_3$.

[a] Department of Chemistry, Durham University, Science Site, Durham DH1 4QG, UK.
[b] Institut Laue Langevin, 71 Avenue des Martyrs, 38000 Grenoble, France.
[c] Diamond Light Source, Harwell Science and Innovation Campus, UK.

Oxide ion transport in apatites has been found experimentally to be highly anisotropic, with the *c*-direction conductivity measured on single crystals being several orders of magnitude higher than that in *a*- and *b*-directions. [16, 34, 35] The precise mechanism of oxide ion conductivity in apatite materials, however, is highly debated in the literature, and appears largely dependent on the identity of the T atom (either Si or Ge). Different oxide ion migration pathways have been proposed. One occurs down the hexagonal channels, *via* an interstitialcy mechanism involving O4 atoms and interstitial oxygens residing in the channel, whose positions were confirmed by neutron power diffraction.[36] This has shown to be the case for $La_{9.33}Si_6O_{26}$ studied using both classical defect energy calculations[25] and density functional theory (DFT)-based nudged elastic band methods.[26] The latter method has also shown the same mechanism for $La_{10}Si_6O_{27}$.[37] An alternative proposed for $La_{9.33}Si_6O_{26}$ is an interstitial mechanism with a complex sinusoidal motion through the hexagonal channel representing the lowest energy pathway through classically calculated potential energy surface.[38, 39] For the germanate materials, interstitial O atoms have been found (computationally and experimentally) on the O5 sites between pairs of GeO_4 polyhedra.[28, 30] Diffusion can then occur in the *c*-direction, either directly between these O5 sites, as found by Kendrick *et al*. for $La_{9.33}Ge_6O_{26}$ using classical molecular dynamics and potential energy surfaces,[40] or between the O5 sites and an oxygen site on a GeO_4 polyhedron, as found by Imaizumi *et al*. in their *ab initio* molecular dynamics (AIMD) study on $La_{10}Ge_6O_{27}$.[27] The movement of oxide ions from the O4 sites to the GeO_4 framework and vice versa, has also been observed, acting as a 'feeder' for *c*-direction diffusion through the framework.[27, 40] Finally, conduction pathways between channels, roughly in the *ab* plane, have been also proposed in both lanthanum silicates[37, 38] and germanates.[27]

Based on the existing body of literature, it seems likely that multiple mechanisms might occur within the same material, with the relative contribution and importance of the different pathways varying depending on composition and temperature. This is supported by classical molecular dynamics simulations carried out on $La_8Y_2Ge_6O_{27}$ by Panchmatia *et al.* which showed that all the oxide ions in this material are mobile, with multiple mechanisms occurring in both the *c*-direction and *ab* plane.[41] The AIMD calculations carried out on $La_{10}Ge_6O_{27}$ by Imaizumi *et al.* at 1750 and 2000 K also showed contributions from three mechanisms, although a cooperative *c*-direction mechanism through the GeO_4 framework dominated.[27] This work was followed up with a first principles study using the nudged elastic band method which showed that this mechanism has the lowest activation energy and is more favoured than a purely interstitial mechanism.[42]

In this paper we report the first AIMD simulation study of the conduction mechanisms in Bi(III)-containing apatite-type oxide ion conductors, performed on the series $La_{10-x}Bi_xGe_6O_{27}$ (x=0, 2, 4) and supported by neutron scattering experiments. We explore the effects that the introduction of this lone-pair species has on the oxide conduction mechanisms and the overall conductivity.

Experimental

Sample Preparation

A 5 g sample of $Bi_2La_8Ge_6O_{27}$ was prepared from stoichiometric amounts of La_2O_3 (Acros Organics, 99.9%), Bi_2O_3 (Acros Organics, 99.9%) and GeO_2 (Acros Organics, 99.999%). The reactants were thoroughly mixed and ground together, placed in an alumina crucible and fired at 1100 ˚C for 36 hours with intermediate grinding and heating and cooling rates of 10 ˚C min^{-1}. Sample purity was confirmed by X-ray diffraction (Fig. S1), using the Rietveld method implemented in Topas Academic. [43, 44]

Neutron Scattering

Neutron scattering data were collected on time-of-flight spectrometer IN6 at the Institut Laue Langevin (ILL) with an incident neutron wavelength of 5.1 Å. The $Bi_2La_8Ge_6O_{27}$ sample was placed in a cylindrical Nb sample holder and data were collected at 800 °C with a collection time of 6.5 hours. Data were also collected on a vanadium sample at 20 °C for 6 hours for use in normalisation. The data were analysed using the LAMP software.[45]

Computational

All calculations were performed on 1 × 1 × 2 supercells of $La_{10}Ge_6O_{27}$, $Bi_2La_8Ge_6O_{27}$, and $Bi_4La_6Ge_6O_{27}$ based on the triclinic $Bi_2La_8Ge_6O_{27}$ model described by Tate et al.[30] Interstitial oxygen atoms positions were chosen at random from the available O5 sites to ensure the correct stoichiometry and the full site occupancy. The locations of the Bi atoms were also chosen randomly from the available La2 sites to match the required stoichiometry. Before any other calculations occurred all structures underwent geometry optimisation in order to reduce the forces on the atoms.

Ab-initio molecular dynamics (AIMD) calculations were carried out using DFT methods implemented in the VASP code[46]. PAW pseudopotentials[47] were used with GGA-PBE functionals.[48] The electronic structure was sampled only at the gamma point. AIMD calculations were performed at 1000 K, 1500 K, 1750 K and 2000 K in the NVT ensemble. These temperatures were chosen for direct comparison with the work of Imaizumi *et al.*,[27] and due to the relatively small number of atoms being probed. For each simulation 60,000 steps of 3 fs were calculated, giving a total of 180 ps of simulation time. Mean square displacements (MSD) and density of states (DOS) were calculated using the MDANSE code,[49] and cloud plots for trajectory visualisation were produced using LAMP.[45]

Results and Discussion

Density of States from Neutron Scattering and Ab Initio Molecular Dynamics

Fig. 2 shows the density of states of $Bi_2La_8Ge_6O_{27}$ measured on IN6 at 800 °C (where appreciable conductivity was observed experimentally) compared with the density of states calculated from AIMD simulations at 1500 K (the lowest simulated temperature where appreciable oxide ion dynamics were observed, *vide infra*). The positions of the three main features

View Article Online
DOI: 10.1039/C8TA00546F

are in good agreement. The relative intensity of the high energy feature is lower in the experimental DOS, consistent with previous studies on oxide ion conductors. This is likely due to low population of high-energy phonons at the measured temperature and applying the Bose population factor to a weak signal.[50, 51] The agreement between the experimental and calculated DOS plots supports the validity of our AIMD simulations and provides evidence that conclusions drawn from them are reliable.

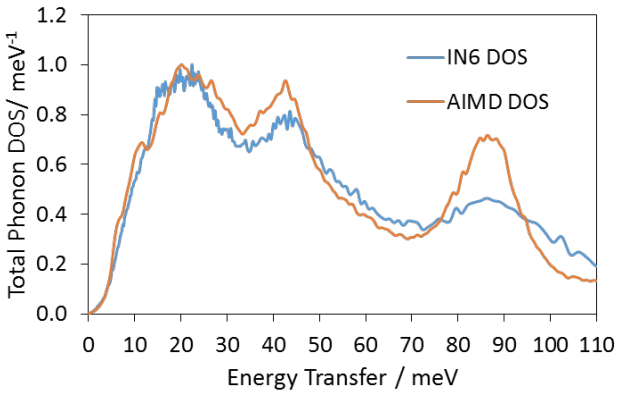

Figure 2. Phonon DOS of $Bi_2La_8Ge_6O_{27}$ calculated from AIMD at 1500 K compared with experimental results from IN6 neutron scattering. The calculated curves have been weighted according to neutron scattering power of Bi, La, Ge, and O and both curves have been scaled to reach a maximum value of 1.

Conduction Mechanisms Investigated by *Ab Initio* Molecular Dynamics

Simulations at 1000 K showed no diffusion events, with all oxygen atoms remaining in their initial sites, in agreement with the behaviour found by Imaizumi *et al*.[27] By contrast, long range diffusion was observed at the three higher temperatures.

Figure 3 shows the mean squared displacement (MSD) of oxygen atoms in the three simulated compositions at each temperature. The MSDs shows no sign of plateauing, indicating that the motion is diffusional rather than being due to the local thermal vibrations of the O atoms. The maximum O^{2-} displacements increase progressively with increasing simulation temperatures, from about 2.3 Å at 1500 K to about 3.5 Å at 1750 K and to about 5 Å at 2000 K. A distance of 2.3 Å is slightly larger than the distance from the O sites in the GeO_4 tetrahedra to the O5 sites (~2.2 Å), whereas 3.5 Å is significantly larger than that between the O sites in the GeO_4 tetrahedra (2.7-2.8 Å). This indicates significant long range diffusion in the material. The plots in Figure 3 show that the MSDs decrease with increased Bi content at 1500 K; however, at higher temperatures the opposite occurs, with the MSDs increasing with Bi content. The simulations at the two higher temperatures are therefore consistent with the experimental findings.[31]

In the course of the higher temperature AIMD simulations four clearly distinct oxide ion exchange mechanisms were observed for all compositions. These are shown in Fig. 4. The simulations at 1500 K show only two of the mechanisms, one involving the movement of oxygen atoms through the GeO_4 framework via the O5 sites (mechanism 1, Fig. 4a), and the other involving oxygen atoms moving from the GeO_4 network into and out of the hexagonal column containing the O4 sites (mechanism 2, Figs. 4a, 4b and 4c). Additionally, in the higher temperature simulations, two further mechanisms were observed. One involves oxide ion exchanges, in the *ab* plane, between the columns formed by the GeO_4 tetrahedra running down the *c*-axis (mechanism 3, Figs. 4b and 4c). The final mechanism involves oxide ion transport in the *c*-direction *via* the O4-containing hexagonal column (mechanism 4, Fig. 4b). Mechanisms 1, 2 and 3 were observed by Imaizumi *et al*. and referred to as the "cooperative *c* axis", "cooperative O4", and "cooperative *ab* plane" mechanisms; mechanism 4 was not observed in their work.[42]

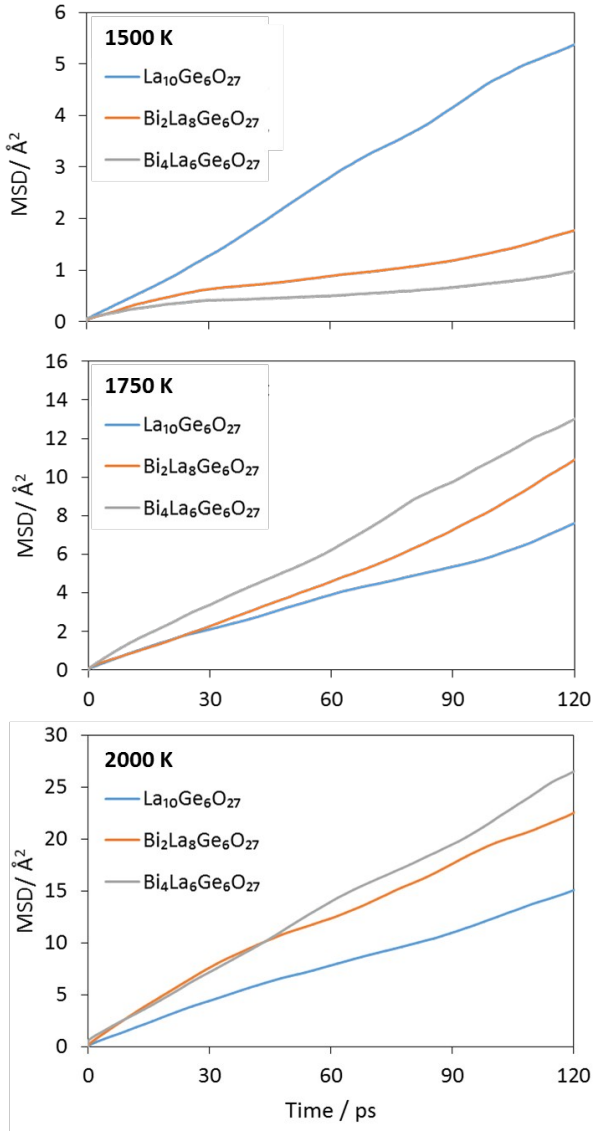

Figure 3: Mean square displacements calculated for $La_{10}Ge_6O_{27}$, $Bi_2La_8Ge_6O_{27}$, and $Bi_4La_6Ge_6O_{27}$ over the course of 120 ps of simulation time at 1500 K, 1750 K and 2000 K.

View Article Online
DOI: 10.1039/C8TA00546J

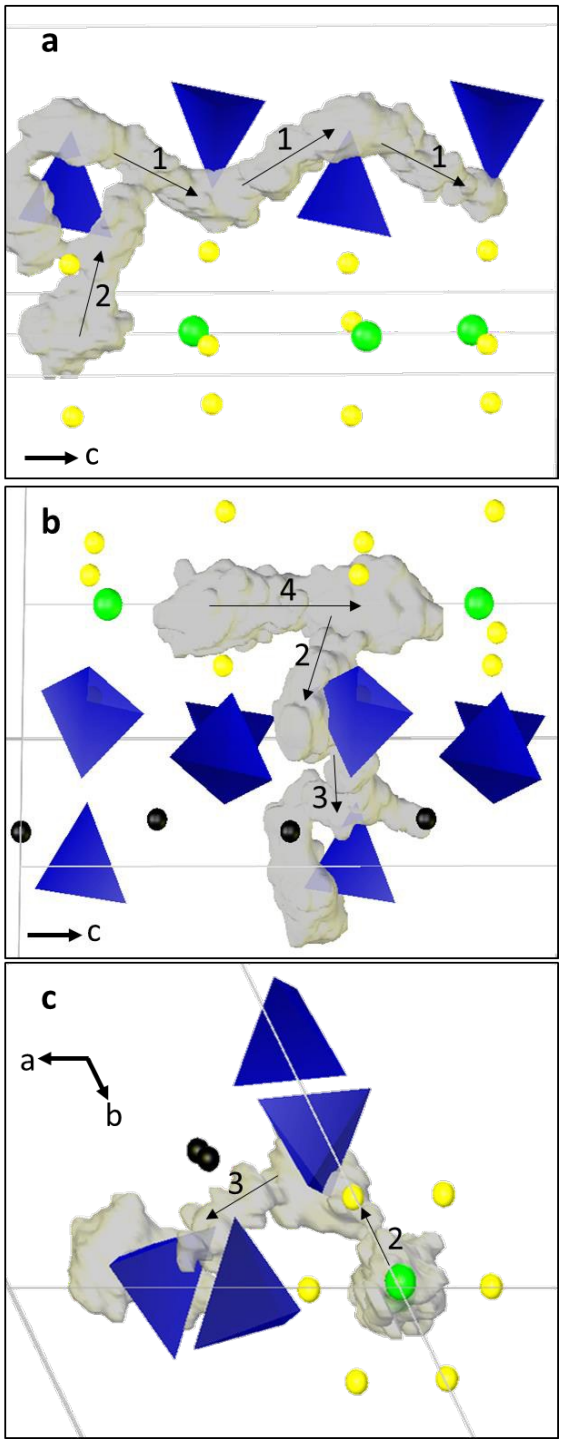

Figure 4: Cloud plots illustrating the four mechanisms of oxide ion conduction observed over the course of AIMD simulation on $La_{10}Ge_6O_{27}$ at 2000 K. Blue tetrahedra are GeO_4, green atoms are O4, yellow atoms are La2 and black atoms are La1. The grey clouds are regions visited by an oxygen atom over the course of the simulation.

Table 1 shows the number of times each exchange mechanisms was observed over the course of each of the simulations, grouped by temperature and composition. For mechanisms 1 and 3, one instance was counted as when an O atom moved from the coordination sphere of one Ge centre to that of another; in other words, O atom jumps within a GeO_4 tetrahedron or jumps to a vacant O5 site were not counted. One instance of mechanism 2 was counted as a movement between an O4 site and the GeO_4 framework or vice versa. An instance of mechanism 4 was counted when an O moved from one O4 to another.

In agreement with the MSD curves shown in Fig. 3, the total number of conduction events decreases significantly with increasing doping level in the 1500 K simulations and increases with increasing Bi content at the higher temperatures. In agreement with literature[27, 28] diffusion *via* the GeO_4 framework (mechanism 1) is the dominant conduction mechanism at all temperatures.

The reduced oxide ion mobility with increasing Bi-content at 1500 K may be due to steric hindrance caused by the Bi lone pair pointing towards the GeO_4 framework[52] and therefore adversely affecting mechanism 1, dominant at this temperature (Fig. 4a, Table 1). A lone pair has similar size to an O^{2-} ion[53, 54] and similar physical blocking of conduction pathways has been offered as an explanation for reductions in conductivity on Bi-doping observed in $La_2Mo_2O_9$.[55, 56]

The relative number of instances of mechanisms 2 and 3 increase with temperature, whereas mechanism 4 seems to only be activated significantly at the highest temperature simulated. The number of instances of all activated oxide ion diffusion mechanisms increase with Bi content at the two highest temperatures. However, the relative proportion of the total diffusion events attributed to mechanism 1 decreases with Bi content, from 69 % to 50 % at 1750 K, and 46 % to 36 % at 2000 K. This may indicate that although a small steric hindrance on mechanism 1 caused by the lone pair remain at these temperatures, this mechanism no longer dominates as the contribution of the other three becomes more prominent. This increase in the relative contributions of the two *ab*-plane conduction mechanisms (2 and 3), indicate that the oxide ion conductivity of Bi-doped apatites could be more isotropic than the parent compounds, which could be important in certain applications.

The fact that at 1500 K we observe only mechanisms 1 and 2, with 3 being seen only at higher temperatures, agrees with the behaviour reported by Imaizumi *et al*.[27] It is also consistent with the relative activation energies found in that work, with an activation energy of 1.17 eV found for mechanism 3, versus 0.64 eV and 0.76 eV for mechanisms 1 and 2, respectively. Mechanism 4 was not observed by Imaizumi *et al.* in their simulations, and while it was only rarely seen in our AIMD simulations at higher temperatures, our results indicate that some conduction directly down the O4-containing hexagonal channel in this way is possible in apatite-type germanates. While oxide ion transport directly down the O4 channel has been previously suggested in silicate apatites, many of these examples involve interstitial O sites within the channel itself.[25, 26, 37, 38] By contrast, our simulations show a vacancy mechanism *via* only O4 sites with vacancies created by mechanism 2, as has been proposed for the apatite-type silicate $La_{9.69}(Si_{5.70}Mg_{0.30})O_{26.24}$.[57]

View Article Online
DOI: 10.1039/C8TA00546J

Table 1: Number of instances of each oxide ion conduction mechanism observed in a 180 ps AIMD simulation at 1500 K, 1750 K and 2000 K for $La_{10-x}Bi_xGe_6O_{27}$ (x=0, 2, 4).

Mechanism	Number of Jumps								
	1500 K			1750 K			2000 K		
	x=0	x=2	x=4	x=0	x=2	x=4	x=0	x=2	x=4
1	21	11	3	24	31	44	40	46	50
2	7	5	4	8	16	26	29	33	40
3	0	0	0	2	8	17	10	24	35
4	0	0	0	1	0	1	8	8	12
Total	28	16	7	35	55	88	87	111	137

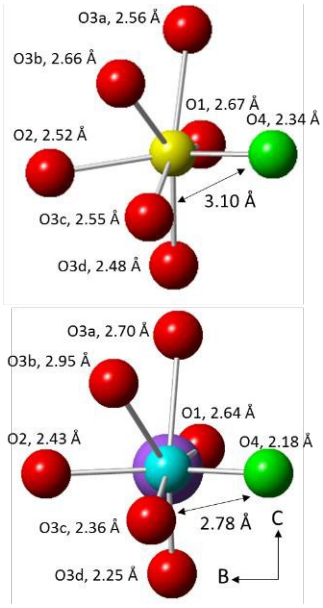

Figure 5: Comparison of the local environments around an A2 La site in $La_{10}Ge_6O_{27}$ (top) and an A2 Bi site in $Bi_2La_8Ge_6O_{27}$ (bottom). The yellow atom is La, blue is Bi, green is O4 and red are other O atoms. The purple region indicates the orientation of the Bi lone pair. [52]

One factor promoting diffusion on the introduction of Bi(III) could be the change in the coordination environment of the A2 sites due to the presence of the lone pair. Fig. 5 shows, as a typical example, the differences in environment of a La atom in $La_{10}Ge_6O_{27}$ and a corresponding Bi atom in the same position in $Bi_2La_8Ge_6O_{27}$ after geometry optimisation; bond length distributions for all Bi and the equivalent La atoms are given in the ESI. It can be seen that four of the Bi-O bonds, including Bi-O4, get shorter in comparison to the equivalent La-O bonds, while two get longer. The shortening of the bonds to O4, O3c and O3d has the effect of bringing key oxygen sites involved in mechanism 2 closer together, which would make the O^{2-} jumps between these sites easier. The reduction of the distance between sites is especially notable in the case of the O4 atom and its nearest neighbour O3c, for which the distance changes from approximately 3.1 Å to around 2.8 Å, and for the next nearest neighbour O3d for which the distance changes from 3.6 to 3.2 Å, a distance that makes movement between these sites much more feasible. Similar changes in the bonding pattern, typical for the introduction of a lone-pair cation, are seen for all La/Bi pairs of corresponding sites (see Fig. S2in ESI), and are likely responsible for the large increase in instances of mechanism 2 upon Bi-doping at higher temperatures.

Another factor is the apparent relative weakness of Bi-O bonds compared to the equivalent La-O bonds. Table S1 shows the calculated Mulliken bond populations[58-60] for the La-O and Bi-O bonds in equivalent A2 sites in $La_{10}Ge_6O_{27}$ and $Bi_2La_8Ge_6O_{27}$. The Mulliken bond population represents the overlap of electronic orbitals between the atoms, where a value of 1 indicates maximum overlap and 0 indicates a non-bonding interaction and a negative value an antibonding state.[61]

Low values have been shown to correlate with the ease of defect formation and oxide ion mobility in fast ion conductors.[62-64] It can be seen from Table S1 and Figure S3 that for most Bi-O bonds the Mulliken populations are lower than for the equivalent La-O bonds. This suggests that the bonds around the Bi sites are apparently weaker and thus oxide ion mobility is facilitated in the doped materials. This decrease in orbital overlap is especially pronounced for the bonds to the O1 and O3a atoms, which are those on the same side of the Bi atom as the lone pair, with changes for the O3b and O3c atoms that are opposite it being much smaller. This suggest that it is repulsion caused by the lone pair introduced on Bi^{3+} that helps increase the oxide ion mobility.

Conclusion

Ab initio molecular dynamics calculations have been used to investigate the effects of doping $La_{10}Ge_6O_{27}$ with lone pair-containing Bi(III) on the individual oxide ion diffusion mechanisms that contribute to the overall conductivity. The simulations show that doping with the lone pair cation increases the overall mobility of oxygen, corroborating experimental results. We have observed four oxide ion exchange mechanisms, and shown that the dominant one is that involving oxide ion transport in the *c*-direction via the GeO_4 network; however, Bi(III)-doping increases the relative proportion of two mechanisms that transport oxide ions in the *ab* plane. This

indicates that doping with lone pair cations could aid in promoting isotropic oxide ion mobility in apatites, a useful feature for some applications. We have also shown the presence of a fourth conduction mechanism at high temperatures, previously not identified in lanthanum germanate apatites, involving conduction down the hexagonal channels in the *c*-direction.

The increased conductivity observed in Bi-doped $La_{10}Ge_6O_{27}$– based materials appears to be a combination of several factors. The first is the change in coordination environment around the channel cation sites (A2) caused by the introduction of the lone pair. The shortening of some bonds and lengthening of others reduces the distance between the channel O4 atoms and their nearest neighbours in the GeO_4 network, significantly easing transport between the channel and the network. The transport is further facilitated by the apparent relative weakness of some Bi-O bonds compared to the equivalent La-O counterparts, as measured by the Mulliken overlap population.

Conflicts of interest

There are no conflicts to declare.

Acknowledgements

The authors thank Durham University and Institut Laue Langevin for a PhD studentship for J. R. P, and Durham University and Diamond Light Source for a PhD studentship for M. S. C. *Email - **ivana.radosavljevic@durham.ac.uk**

Notes and references

1. D. Yuan and F. A. Kröger, *Journal of The Electrochemical Society*, 1969, **116**, 594-600.
2. J. Sunarso, S. Baumann, J. M. Serra, W. A. Meulenberg, S. Liu, Y. S. Lin and J. C. Diniz da Costa, *Journal of Membrane Science*, 2008, **320**, 13-41.
3. P. N. Dyer, R. E. Richards, S. L. Russek and D. M. Taylor, *Solid State Ionics*, 2000, **134**, 21-33.
4. E. D. Wachsman and K. L. Duncan, *Ceria/bismuth oxide bilayered electrolytes for low temperature solid oxide fuel cells*, Electrochemical Society Inc, Pennington, 1999.
5. S. J. Skinner and J. A. Kilner, *Materials Today*, 2003, **6**, 30-37.
6. D. J. L. Brett, A. Atkinson, N. P. Brandon and S. J. Skinner, *Chem. Soc. Rev.*, 2008, **37**, 1568-1578.
7. F. Shimojo and H. Okazaki, *Journal of the Physical Society of Japan*, 1992, **61**, 4106-4118.
8. Y. Yamamura, S. Kawasaki and H. Sakai, *Solid State Ionics*, 1999, **126**, 181-189.
9. M. Nakayama, H. Ohshima, M. Nogami and M. Martin, *Physical Chemistry Chemical Physics*, 2012, **14**, 6079-6084.
10. X. Kuang, J. L. Payne, M. R. Johnson and I. R. Evans, *Angew. Chem. Int. Edit.*, 2012, **51**, 690-694.
11. X. Kuang, J. L. Payne, J. D. Farrell, M. R. Johnson and I. R. Evans, *Chem. Mater.*, 2012, **24**, 2162-2167.
12. J. L. Payne, M. G. Tucker and I. R. Evans, *J. Solid State Chem.*, 2013, **205**, 29-34.
13. J. L. Payne, J. D. Farrell, A. M. Linsell, M. R. Johnson and I. R. Evans, *Solid State Ionics*, 2013, **244**, 35-39.
14. M. S. Islam, J. R. Tolchard and P. R. Slater, *Chem. Commun.*, 2003, DOI: 10.1039/b301179h, 1486-1487.
15. H. Arikawa, H. Nishiguchi, T. Ishihara and Y. Takita, *Solid State Ionics*, 2000, **136**, 31-37.
16. S. Nakayama, M. Sakamoto, M. Higuchi, K. Kodaira, M. Sato, S. Kakita, T. Suzuki and K. Itoh, *Journal of the European Ceramic Society*, 1999, **19**, 507-510.
17. P. R. Slater, J. E. H. Sansom and J. R. Tolchard, *Chemical Record*, 2004, **4**, 373-384.
18. J. Xiang, Z.-G. Liu, J.-H. Ouyang and F.-Y. Yan, *Journal of Power Sources*, 2014, **251**, 305-310.
19. H. Li, T. Baikie, S. S. Pramana, J. F. Shin, P. J. Keenan, P. R. Slater, F. Brink, J. Hester, T. An and T. J. White, *Inorganic Chemistry*, 2014, **53**, 4803-4812.
20. J. E. H. Sansom and P. R. Slater, *Solid State Ionics*, 2004, **167**, 23-27.
21. E. Kendrick, J. Sansom, J. Tolchard, M. Islam and P. Slater, *Faraday Discussions*, 2007, **134**, 181-194.
22. T. J. White and Z. L. Dong, *Acta. Cryst. B*, 2003, **59**, 1-16.
23. A. Jones, P. R. Slater and M. S. Islam, *Chemistry of Materials*, 2008, **20**, 5055-5060.
24. S. S. Pramana, W. T. Klooster and T. J. White, *Acta Cryst. B*, 2007, **63**, 597-602.
25. E. Bechade, O. Masson, T. Iwata, I. Julien, K. Fukuda, P. Thomas and E. Champion, *Chem. Mater.*, 2009, **21**, 2508-2517.
26. K. Matsunaga and K. Toyoura, *Journal of Materials Chemistry*, 2012, **22**, 7265-7273.
27. K. Imaizumi, K. Toyoura, A. Nakamura and K. Matsunaga, *Solid State Ionics*, 2014, **262**, 512-516.
28. E. Kendrick, A. Orera and P. R. Slater, *Journal of Materials Chemistry*, 2009, **19**, 7955-7958.
29. L. Leon-Reina, J. M. Porras-Vazquez, E. R. Losilla and M. A. G. Aranda, *Solid State Ionics*, 2006, **177**, 1307-1315.
30. M. Tate, D. Blom, M. Avdeev, H. Brand, G. McIntyre, T. Vogt and I. Evans, *Advanced Functional Materials*, 2017, **27**.
31. M. Tate, C. Fuller, M. Avdeev, H. Brand, G. McIntyre and I. Evans, *Dalton Transactions*, 2017, **46**, 12494-12499.
32. J. R. Tolchard, J. E. H. Sansom, P. R. Slater and M. S. Islam, *J Solid State Electrochem*, 2004, **8**, 668-673.
33. L. León-Reina, E. R. Losilla, M. Martinez-Lara, S. Bruque, A. Llobet, D. V. Sheptyakov and M. A. G. Aranda, *Journal of Materials Chemistry*, 2005, **15**, 2489-2498.
34. K. Fukuda, T. Asaka, M. Okino, A. Berghout, E. Bechade, O. Masson, I. Julien and P. Thomas, *Solid State Ionics*, 2012, **217**, 40-45.
35. Y. Kim, D. Shin, E. Shin, H. Seo and J. Lee, *Journal of Materials Chemistry*, 2011, **21**, 2940-2949.
36. L. Leon-Reina, E. R. Losilla, M. Martinez-Lara, S. Bruque and M. A. G. Aranda, *Journal of Materials Chemistry*, 2004, **14**, 1142-1149.
37. K. Imaizumi, K. Toyoura, A. Nakamura and K. Matsunaga, *Journal of Physics-Condensed Matter*, 2015, **27**.
38. E. Kendrick, M. S. Islam and P. R. Slater, *J. Mater. Chem.*, 2007, **17**, 3104-3111.
39. J. Tolchard, M. Islam and P. Slater, *Journal of Materials Chemistry*, 2003, **13**, 1956-1961.

View Article Online
DOI: 10.1039/C8TA00546J

40. E. Kendrick, M. S. Islam and P. R. Slater, *Chemical Communications*, 2008, DOI: 10.1039/b716814d, 715-717.
41. P. Panchmatia, A. Orera, G. Rees, M. Smith, J. Hanna, P. Slater and M. Islam, *Angewandte Chemie-International Edition*, 2011, **50**, 9328-9333.
42. K. Imaizumi, K. Toyoura, A. Nakamura and K. Matsunaga, *Journal of the Ceramic Society of Japan*, 2017, **125**, 105-111.
43. A. A. Coelho, J. S. O. Evans, I. R. Evans, A. Kern and S. Parsons, *Powder Diffraction*, 2011, **26**, S22.
44. H. M. Rietveld, *Journal of Applied Crystallography*, 1969, **2**, 65-&.
45. D. Richard, M. Ferrand, G. and J. Kearley, *Journal of Neutron Research*, 1996, **4**, 33-39.
46. G. Kresse and J. Furthmuller, *Computational Materials Science*, 1996, **6**, 15-50.
47. G. Kresse and D. Joubert, *Physical Review B*, 1999, **59**, 1758-1775.
48. J. Perdew, K. Burke and M. Ernzerhof, *Physical Review Letters*, 1996, **77**, 3865-3868.
49. E. C. Pellegrini, G. Goret and A. Aoun, 2016.
50. J. R. Peet, C. A. Fuller, B. Frick, M. Zbiri, A. Piovano, M. R. Johnson and I. R. Evans, *Chemistry of Materials*, 2017, **29**, 3020-3028.
51. C. D. Ling, W. Miiler, M. R. Johnson, D. Richard, S. Rols, J. Madge and I. R. Evans, *Chem. Mater.*, 2012, **24**, 4607-4614.
52. J. R. Peet, A. Piovano, M. Johnson and I. R. Evans, *Dalton Transactions*, 2017, DOI: 10.1039/C7DT03956E.
53. X. P. Wang, Q. F. Fang, Z. S. Li, G. G. Zhang and Z. G. Yi, *Applied Physics Letters*, 2002, **81**, 3434-3436.
54. P. Moore and J. Shen, *American Mineralogist*, 1984, **69**, 1173-1179.
55. F. Goutenoire, O. Isnard, E. Suard, O. Bohnke, Y. Laligant, R. Retoux and P. Lacorre, *Journal of Materials Chemistry*, 2001, **11**, 119-124.
56. P. Lacorre, F. Goutenoire, O. Bohnke, R. Retoux and Y. Laligant, *Nature*, 2000, **404**, 856-858.
57. R. Ali, M. Yashima, Y. Matsushita, H. Yoshioka, K. Ohoyama and F. Izumi, *Chemistry of Materials*, 2008, **20**, 5203-5208.
58. R. MULLIKEN, *Journal of Chemical Physics*, 1955, **23**, 1833-1840.
59. R. MULLIKEN, *Journal of Chemical Physics*, 1955, **23**, 1841-1846.
60. R. MULLIKEN, *Journal of Chemical Physics*, 1955, **23**, 2338-2342.
61. M. Segall, R. Shah, C. Pickard and M. Payne, *Physical Review B*, 1996, **54**, 16317-16320.
62. K. Nakamura, M. Mori, T. Itoh and T. Ohnuma, *Aip Advances*, 2016, **6**.
63. V. Zainullina and V. Zhukov, *Physics of the Solid State*, 2001, **43**, 1686-1699.
64. Y. Emel'yanova, R. Shafigina, E. Buyanova, V. Zhukovskii, V. Zainullina and S. Petrova, *Russian Journal of Physical Chemistry*, 2006, **80**, 1725-1730.

View Article Online
DOI: 10.1039/C8TA00546J

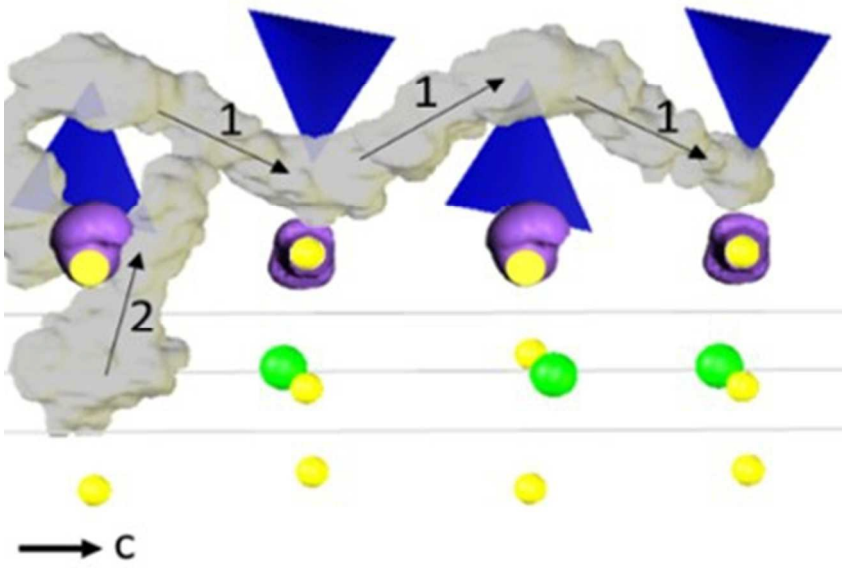

70x51mm (150 x 150 DPI)